Heliyon 9 (2023) e20809

Contents lists available at ScienceDirect

Heliyon

journal homepage: www.cell.com/heliyon

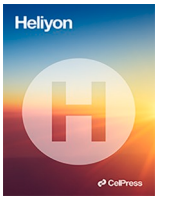

Improvement of the photocatalytic activity of ZnO thin films doped with manganese

William Vallejo *, Alvaro Cantillo, Carlos Díaz-Uribe

Grupo de Fotoquímica y Fotobiología, Facultad de Ciencias Básicas, Universidad del Atlántico, 081007, Puerto Colombia, Colombia

ARTICLE INFO

Keywords:
Environmental remediation
Heterogeneous photocatalysis
ZnO
Metal-doping
Thin films

ABSTRACT

In the herein report, we synthesized ZnO thin films doped with manganese (Mn). We studied the impact of Mn doping loads (1 %, 3 %, 5 % wt.) on physicochemical properties of the compounds. Furthermore, we presented the photocatalytic efficiency in removal of methylene blue dye. The structural assay indicated ZnO conserve the wurtzite crystalline structure after dopant insertion. Furthermore, the crystalline size of catalysts was reduced after dopant incorporation. The SEM analysis showed a change in surface morphology after modification of ZnO thin films. Furthermore, Raman spectroscopy verified the Mn insertion inside the ZnO lattice. After the doping process, band gap was reduced by 16 %, in comparison to bare ZnO. After the photocatalytic test, the doped catalysts showed better performance than bare ZnO in removing MB. The best test showed a kinetics constant value of 2.9×10^{-3} min^{-1} after 120 min of visible irradiation. Finally, the Mn(5 %):ZnO thin film was suitable after five degradation cycles, and the degradation process efficiency was reduced by 32%.

1. Introduction

In the last decades, water remediation using heterogeneous photocatalysis (HP) has grown due to its efficacy in removing emerging pollutants (e.g., pharmaceuticals, pesticides, fertilizers, and dyes) [1–3]. The HP physical process relies on semiconductor activation by electromagnetic radiation absorption, then the electrons and holes can be generated, after that the reactive oxidative species (ROS) can be produced on catalyst surface, and these ROS can degrade emerging pollutants [4]. Nowadays, TiO_2 is the main photocatalyst studied for environmental applications [5,6].

The HP degradation tests are commonly performed in suspension (e.g., catalysts as nano-powders in suspension); however, practical problems can arise (e.g., separation of the semiconductor after the degradation process is finished). This is a drawback when HP are incorporated in a continuous flow system [7,8]. However, anchoring the semiconductor to a surface (e.g., thin films, coatings) can solve these problems. The semiconductors can be deposited as thin films by various methods, namely: (i) physical (e.g., pulsed-laser deposition [9], sputtering [10], reactive evaporation [11], thermal evaporation [12] and, atomic layer deposition [13], ultrasonic and microwave-assisted methods [14]); (ii) chemical (e.g., electrochemical [15], chemical vapor deposition [16], SILAR technique [17], chemical bath deposition (CBD) [18], and sol-gel method [19]).

Hassan et al. reported that about 190 semiconductors have been studied to develop photocatalytic applications. Fig. 1 compares the band gap value of various semiconductors against a normal hydrogen electrode (NHE) [20]. Among these semiconductors, ZnO is

* Corresponding author.
E-mail address: williamvallejo@mail.uniatlantico.edu.co (W. Vallejo).

https://doi.org/10.1016/j.heliyon.2023.e20809
Received 29 April 2023; Received in revised form 7 September 2023; Accepted 6 October 2023

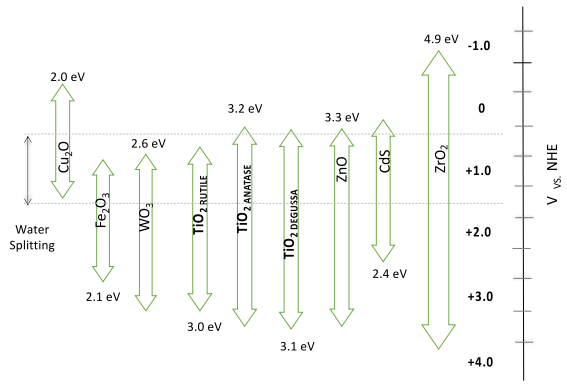

Fig. 1. Band gap semiconductors against NHE redox potential.

commonly used in HP due its physical and chemical properties (e.g., stability, low toxicity, mobility of charge carriers) [21]. However, this semiconductor is effective in photocatalytic application only at the ultraviolet range of the electromagnetic spectrum [22]. Various strategies have been applied to solve these issues, such as: (i) quantum dots [23]; (ii) heterojunctions with other semiconductors [24]; (iii) (iv) sensitization [25–27]; (v) composites with inorganic compounds [28]; surface plasmon resonance [29] and (vi) doping and co-doping [30]. Among these strategies, the doping method is implemented to change band gap values (E_g) and catalytic properties of semiconductors [31].

Different transition metals have been employed to dope ZnO [32–35]. Manganese, an abundant element on Earth (i.e., it is second only to iron among the transition elements in abundance) and it is unexpensive compared to other transitions elements; besides, this element is an essential element for many biological process [36,37]. Furthermore, the ion Mn(II) radius is smaller than that of Zn(II), making the doping process easier. Mn-doped ZnO has been successfully prepared by different techniques (e.g., RF Magnetron sputtering [38], solution combustion technique [39], sol-gel [40], ultrasonic spray pyrolysis [41], spray pyrolysis [42] and co-precipitation [43]). Among these synthesis procedures, the sol-gel method at low temperatures is very attractive because it is inexpensive, and its implementation does not demand difficult experimental conditions as physical methods do [44]. The doping process as an alternative for modifying the chemical and photophysical properties of semiconductors is a common method used in HP applications, the doping process is determined by experimental condition (e.g., reagent concertation, pH, temperature, stirring) [45]. Das et al. verified an enhancement of removal efficiency of ZnO as result of doping with manganese [46]. Qi et al. studied the performance of ZnO after doping it with five metals using the solvothermal method. In their study, the Mn-doped ZnO samples reached the second-best photodegradation value [35]. Other type of dyes are studied as pollutant models; Singh et al. degraded methyl orange using ZnO doped with manganese as photocatalyst [47]. Insertion of Mn inside the oxide semiconductor lattice can change their physical and chemical properties (e.g., structural, morphological, optical), and all these changes can modify the photocatalytic properties of semiconductor towards lower energy (e.g., visible region of spectrum).

In this contribution, we reported the impact of Mn-doping process in physical and photocatalytic properties of ZnO.

2. Materials and methods

2.1. Synthesis and characterization of the catalysts

We utilized sol-gel technique to obtain both bare ZnO and doped materials. Details of the synthesis process in a previous report [48]. To obtain Mn-doped ZnO powder, Mn^{2+} ions were added during ZnO synthesis using $MnSO_4$ (Merck) as manganese source. The doping loads of ZnO were set at 1.0%, 3.0%, 5.0 % wt. Details of quantification Mn loads in the supporting information. We utilized soda-lime glass substrate (2 cm × 2 cm) to immobilize powders using the Doctor Blade method. Procedural details can be reached in a previous report [49]. The physical chemical properties were determined through Raman spectroscopy, Diffuse Reflectance, X-ray diffraction and scanning electron microscopy for using DXR device equipped with a 780 nm laser, Thermo Scientific Evolution 220 spectrophotometer, X-ray diffractometer Shimadzu 6000 (Cu Kα radiation) and SEM instrument model QUANTA FEG 650 respectively.

2.2. Photocatalytic study

The thin films (0.100 g catalysts) were immersed into 50 mL of aqueous solution ([MB] = 10 mgL^{-1}, pH = 7.0) in a batch reactor for 60 min at 100 rpm. After that, the reactor was irradiated using visible radiation for 120 min (we used a Light Emitted Diode tape as electromagnetic source, cold white light at 17 W). The amount MB was quantified by spectrophotometry (calibration curve fitting R = 0.998). We applied the Langmuir-Hinshelwood kinetics fitting to study the photocatalytic process according to Ref. [50]:

$$[MB]_t = [MB]_o e^{-k_{ap} t} \quad (1)$$

where $[MB]_t$ is methylene blue concentration of at every time during the photocatalytic process, (t) corresponds to time of irradiation,

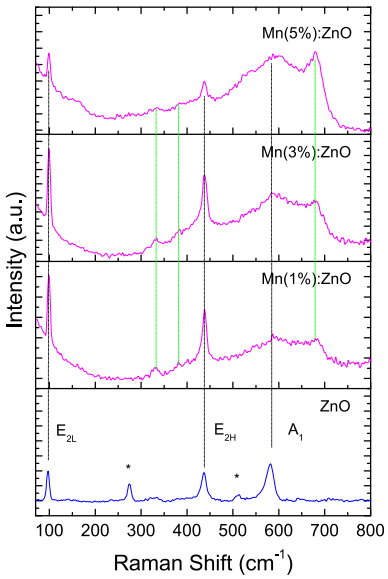

Fig. 2. Raman spectrum of the catalysts fabricated.

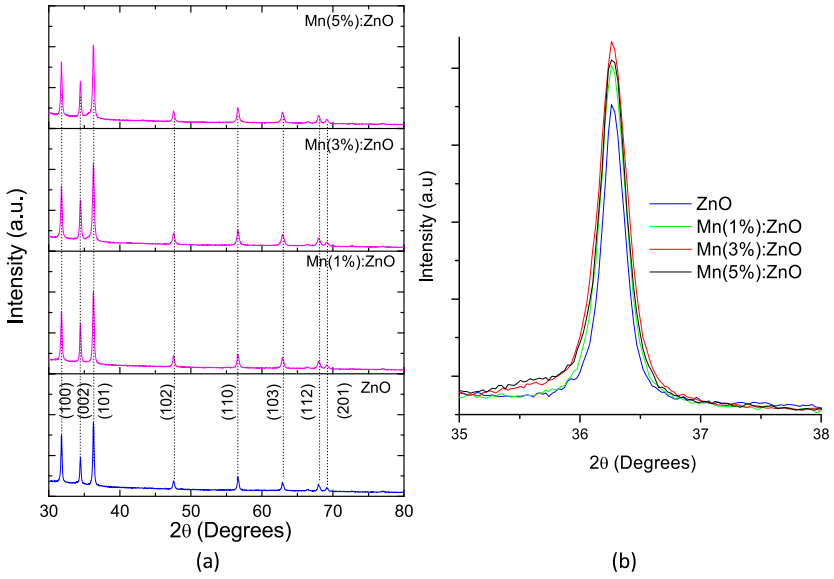

Fig. 3. (a) XRD patterns for the catalysts' thin films, showing planes of each signal (JCPDS No. 36−1451); (b) Comparison of plane (101).

k_{ap} is the kinetic constant (min^{-1}).

3. Results and discussions (1)

3.1. Spectroscopic assay

Three vibrational modes have been reported for ZnO, of which only two are Raman-active modes [51]. Fig. 2 shows Raman spectra for the catalysts. Results show typical signals for the ZnO semiconductor, where normal modes at 97.4, 437.0, and 581.1 cm^{-1} correspond to E_{2L}, E_{2H} and A_1, respectively [52]. Fig. 2 shows two new optical modes at 274.4, and 512.6 cm^{-1}, some authors assigned these signals to introduction of nitrogen inside the ZnO lattice [53,54]. Other reports suggest these signals can appear without presence of nitrogen. Friedrich et al. suggested the presence of interstitial Zn (Zn_i) when those vibrational modes appear in spectrum for using Raman spectroscopy with ab initio calculations on ZnO layers [55,56]. Wang et al. reported that such signals can be induced by ZnO

Table 1
Results of X-ray analysis for catalysts.

Catalyst	Crystalline size (nm)	$\varepsilon \times 10^{-3}$	$\Delta\varepsilon$ (%)	δ x10^{14} (lines/m^2)
ZnO	34.9	0.9987	–	8.2
Mn(1 %):ZnO	31.4	1.1107	11.2	10.15
Mn(3 %):ZnO	29.8	1.1701	17.16	11.26
Mn(5 %):ZnO	31.5	1.1074	10.89	10.09

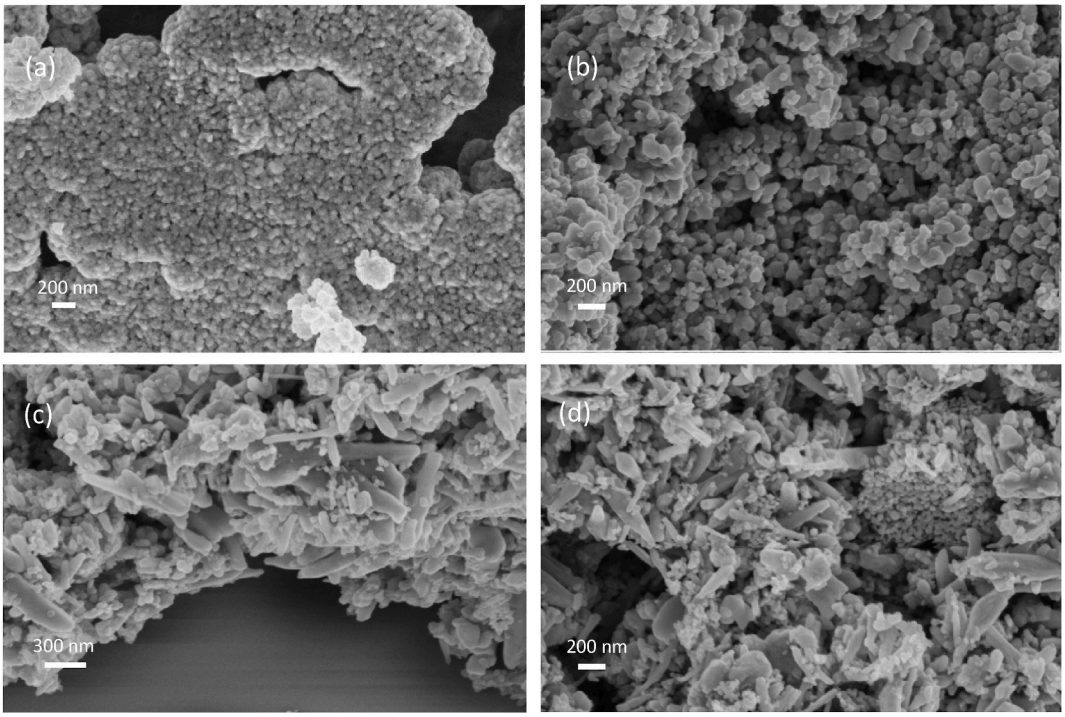

Fig. 4. Scanning Electron Microscopy images: (a) ZnO; (b) Mn(1 %):ZnO; (c) Mn(3 %):ZnO and, (b) Mn(5 %):ZnO (x 26000).

defects (e.g., Zn_i) [57]. No signals corresponding to the MnO_x phase are observed in the Raman spectrum [58]. However, new phonon bands appear in Fig. 2 for doped ZnO samples (green dot line in Fig. 2) which are characteristic of spinel structure $ZnMn_2O_4$. It is possible this phase ZnO–Mn could be generated on thin films surface [59,60].

3.2. Structural characterization

Fig. 3(a) shows the structural characterization. Results shows that ZnO was polycrystalline, and the peak located at $2\theta = 36.27$ corresponds to the preferential plane growth (PPG) (101), in addition, the X-ray pattern shows typical signals for ZnO, and all these reflections correspond to the wurtzite phase with hexagonal crystalline structure [61]. After the doping process, the X-ray of Mn-doped ZnO showed the same signals as those of bare ZnO. Fig. 3(a) does not show other signals corresponding to MnOx phases. However, most diffraction patterns decreasing the intensity signal of the PPG after the doping process, (Fig. 3(b)); this result suggests that the ions of the metals could have managed to replace Zn(II) inside ZnO lattice. Similar results were reported before for $Zn_{1-x}Mn_xO$ [62–64]. This behavior has been associated to a change in oxygen vacancies (VO) and a change in crystalline size [65]. The VO was reported for Mn-doped ZnO coatings deposited by pulsed laser [9,66]. We determined the crystalline properties of materials according to equation (eq. (2)) [67]:

$$D = \frac{C\lambda}{\beta \cos\theta} \tag{2}$$

This is the Scherrer's equation, where D is the crystalline domain size, β is the full width at half maximum of X-ray peak (FWHM) for the highest peak (101), λ is the X-ray wavelength ($\lambda = 0.15406$ nm), θ is the Bragg angle, and C is the correction factor (0.9 in this calculation) [68]. Furthermore, we determined the dislocation density (δ, eq. (3)) and the microstrain value (ε, eq. (4)) for catalysts, according to this equation [69]:

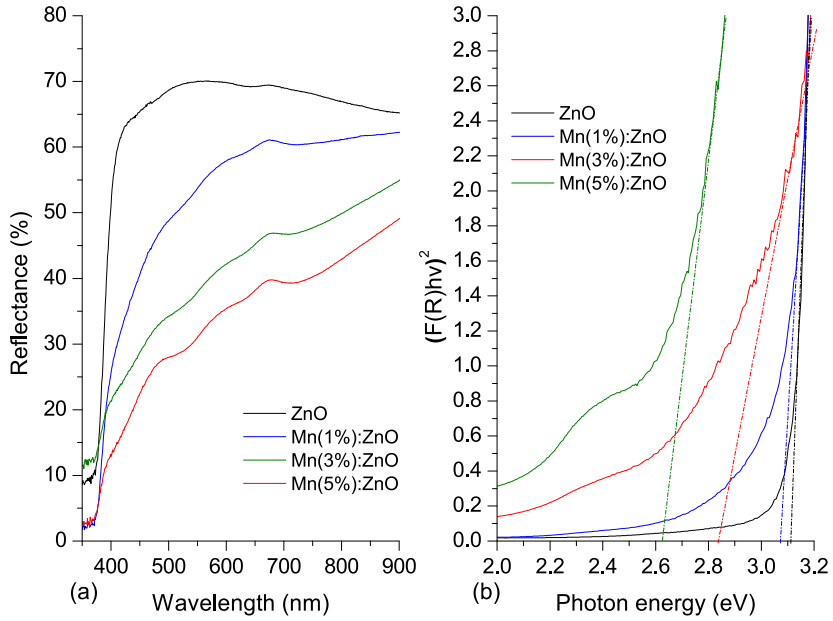

Fig. 5. (a) Reflectance spectra of the catalysts; (b) KM function of the catalysts.

Table 2
E_g value and photocatalytic results of the catalysts.

Thin film	Band gap (eV)[2]	$k_{ap} \times 10^{-3}$ (min^{-1})	half-life time(min)	Degradation (%)
ZnO	3.11	0.2	3465	2.5
Mn(1 %):ZnO	3.04	1.8	385	20.9
Mn(3 %):ZnO	2,82	2.1	330	23.7
Mn(5 %):ZnO	2.62	2.9	239	32.6

$$\delta = \frac{1}{D} \tag{3}$$

$$\varepsilon = \frac{\beta * cos\,\theta}{4} \tag{4}$$

Table 1 lists the crystalline parameters for all catalysts after applied equations (2)–(4). After ZnO was doped with Mn, the PPG was reduced, and the peaks exhibited significant broadening. Such large XRD line broadening in Mn-doped ZnO indicates formation of lattice defects in the thin films [58]. Despite that, signals corresponding to MnOx did not appear in Fig. 3(a). During the chemical synthesis procedure, the chemical phase ZnM_2O_4 could be generated on thin films surface (as Raman's results suggested). Due to reduced load inside ZnO thin films (1.0–5.0 wt%) in the X-ray patterns only change the width of PPG (Fig. 3(b)), the ZnM_2O_4 has a strong signal at $2\theta = 36.4°$, this signal corresponds to plane (211) JCPDS file No. 77–0470 [70]. If ZnM_2O_4 is present in a very small load the signal could be overlapped by the PPG ZnO wurtzite peaks ($2\theta = 36.27°$). Independently of the metal load the crystalline size of thin films was reduced (Fig. 3(b) and Table 1). The differences in the radius between Mn(II) (67 p.m.) and Zn(II) (74 p.m.) can explain this behavior [71]. Table 1 indicates that, regardless of the metal load, the strain of thin films increases between 10.8 and 17.16%, and the dislocation density of the thin films increases between 23 and 37%. The increase in strain is according with increasing of δ, higher strain values suggests higher lattice defects in ZnO [69].

3.3. Morphological study

The SEM images for bare ZnO (Fig. 4(a)) and ZnO doped with three Mn load (4(b):1 %, 4(c):3 % and 4(d):5 % wt.). Results shows bare ZnO is composed of microaggregates (~200 nm) composed of quasi-spherical ZnO nanoparticles (~50 nm); thin films shows of a dense packing of particles. Results shows the surface morphological properties were affected by modification process [72]. The Mn(1 %):ZnO surface consists grains with spherical shape (around ~100 nm). The Mn(3 %):ZnO and Mn(5 %):ZnO thin films are composed of nanorods. Fig. 4(a) - 4(d) shows significative differences in the surface morphology after doping. This behavior indicates the Mn dopant affects the growth mechanism of ZnO thin films [73].

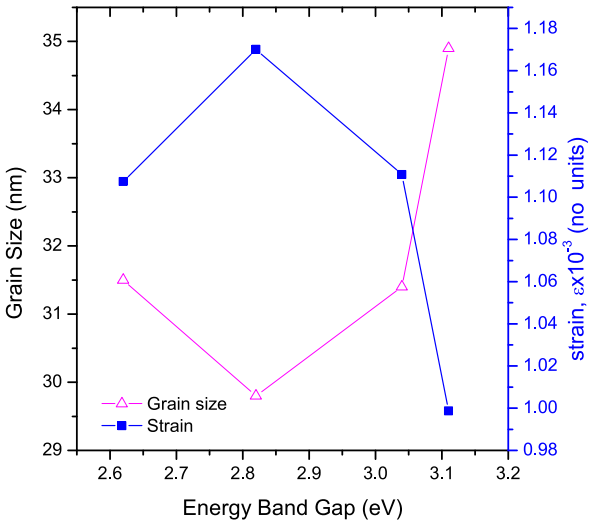

Fig. 6. Strain and crystalline size vs E_g for the catalysts.

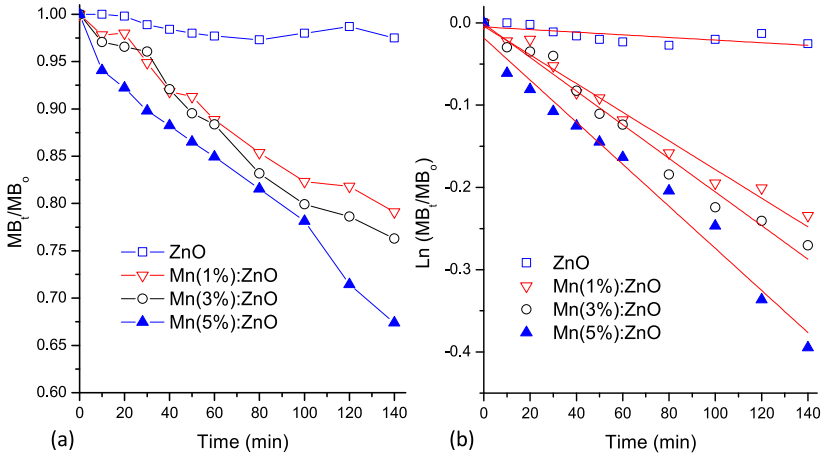

Fig. 7. (a) $[MB]_t/[MB]_o$ vs. time of visible irradiation on the thin films. (b) Langmuir-Hinshelwood fitting.

3.4. Optical characterization

The optical characterization results for the catalysts are shown in Fig. 5(a). ZnO shows a high reflectance at the visible range spectrum. This result agrees with the largest band gap (E_g) of ZnO [74]. Results show that the reflectance films was reduced with the increasing metal amount (Fig. 5(a)). The metal dopant incorporated in the crystal semiconductor can reduce the energy required for the optical transition [75]. Fig. 5(b) shows Kubelka–Munk (KM) model for the catalysts [76]. Furthermore, Table 2 lists the E_g for all materials. The estimated E_g for bare ZnO was 3.11 eV, which is a value in line with previous reports [77]. For doped ZnO, the E_g was smaller than for the bare ZnO (see Table 2), furthermore, the E_g decreased as the dopant's metal content increased. Mn^{2+} has a smaller ionic radius (67 p.m.) than Zn^{2+} (74 p.m.), Mn^{2+} can replace Zn^{2+} inside ZnO. During the doping process, the free Mn^{2+} in the lattice of ZnO was able to create an excited state, and the reduction in the E_g doped thin films could be associated to d-d transition from valence band of ZnO to excited states of Mn^{2+} [78–80]. Finally, the decreas in the E_g value could be the result of VO increasing inside the ZnO lattice after the doping process [81].

Optical characterization is an important property of semiconductors, especially to develop applications in heterogeneous photocatalysis. Fig. 6 shows the relationships among crystalline size, microstrain, and band gap. These results suggest a ratio between decreasing of E_g and mean crystalline size with the increasing in microstrain. The increase in microstrain can be associated to the Manganese load inside the catalyst after modification. This effect changes the crystal size (section 3.2.) and, the lattice parameters across ZnO favored the generation of strain due to the differences between the atomic radius of both elements [82]. The increase in the manganese amount inside the ZnO lattice actives and amplifies the defects in the semiconductor lattice [57].

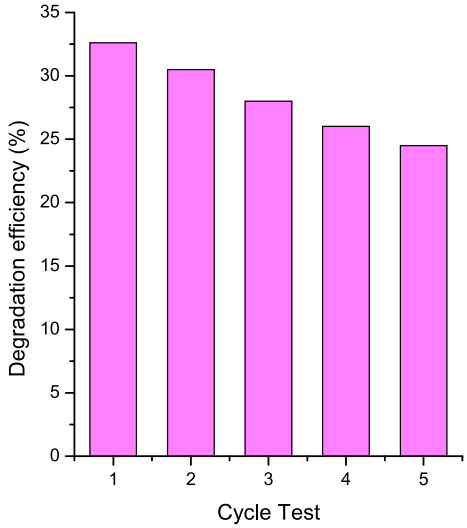

Fig. 8. Stability test of Mn(5 %):ZnO in the MB photocatalytic removal.

3.5. Photocatalytic study

Prior to starting the photodegradation process, reaching the adsorption-desorption on the ZnO surface is required. The adsorption-desorption equilibrium process has been little investigated in photocatalytic studies. In our case, all the samples reached the adsorption-desorption equilibrium at darkness after 60 min. This result is significant because it verifies the need to establish an initial time prior to the photocatalysis process, ensuring that the adsorption-desorption equilibrium is reached. Fig. 7(a) shows the plot of $[MB]_t/[MB]_o$ vs. time of visible irradiation on catalysts, and the Langmuir–Hinshelwood fitting (eq. (1)) is shown in Fig. 7(b). Table 2 lists kinetics parameters after applying the fitting kinetic model. Mn-doped ZnO showed larger efficiency in MB degradation than bare ZnO did (see Table 2). The reduction in the band gap value and the crystalline size can explain these results. The insertion of Mn^{2+} ions can reduce the rate growth of ZnO nanoparticles, generating a smaller particles size (larger surface area), favoring degradation of MB [83]. Furthermore, the reduction in E_g allows that radiation with lower energy values can activate the semiconductor. Fig. 7(a) shows that bare ZnO was not active during visible irradiation. However, the intra-band transitions generated after the doping process reduced the Fermi level of ZnO allow to Mn-doped ZnO be photocatalytic active at the visible range. Mn(5 %):ZnO has the smallest E_g (2.62 eV) and the highest k_{ap} value (2.9×10^{-3} min^{-1}), and the rate of this test was 10 times faster than that for bare ZnO. According to Table 2, the half-life time for the Mn(5 %):ZnO thin films will be 239 min under visible radiation. This is one of the main characteristic modifications of semiconductors because ZnO is not active under visible irradiation. In this case, the main source of energy is visible light (unexpensive and abundant), a critical requirement in the implementation of green strategies of remediation. The k_{ap} values reported (Table 2) are suitable as compared to previous reports. Pérez-Gonzales et al., reported $k_{ap} = 9.9 \times 10^{-3}$ min^{-1} in photodegradation of MB using Ag-loaded TiO_2–ZnO thin films as photocatalyst [84]. Park et al. reported $k_{ap} = 18 \times 10^{-3}$ min^{-1} in the removal of 2,4-dinitrophenol on ZnO functionalized with carbon [85]. Türkyilmaz reported $k_{ap} = 7.5 \times 10^{-3}$ min^{-1} in photodegradation of tartrazine using ZnO doped with Fe [86]. In a previous study, our group reported $k_{ap} = 7.2 \times 10^{-3}$ min^{-1} in photodegradation of MB using ZnO doped with Co [87]. Jayswal reported $k_{ap} = 21.2 \times 10^{-3}$ min^{-1} in removal of Rhodamine-dye using SnS/ZnO heterojunction [88]. Although the k_{ap} values reported in this work are smaller than those reported by other authors, we stand out because in most of those reports the use of the catalyst in suspension affected the implementation of HP in a continuous flow system.

Fig. 8 shows the stability results of the Mn(5 %):ZnO thin films after 5 consecutive photocatalytic cycles. The thin films showed suitable stability, and photocatalytic activity decreased by 32 % after 5 photocatalytic cycles using the same thin films. This behavior is a consequence of both: (i) the physical and chemical stability of the ZnO and (ii) the deposition of the semiconductor as a thin film on a stable substrate (soda-lime glass).

4. Conclusions

We obtained bare ZnO and Mn-doped ZnO (1 %, 3 %, 5 % wt.). We determined physical and chemical properties of the catalysts. Characterization techniques verified the Mn doping process. Results showed a reduction in E_g when the catalysts were doped, and the application of the Scherer equation on XRD patterns indicated a reduction in the crystalline size after the doping process. The increasing in microstrain and decreasing in the band gap value was related with the Mn load inside the ZnO lattice after modification. Mn-doped ZnO showed larger efficiency than ZnO MB removal. The Mn(5 %):ZnO thin films showed the greatest reduction in E_g (2.62 eV) and the highest k_{ap} value (2.9×10^{-3} min^{-1}). Finally, recyclability test suggests that Mn(5 %):ZnO was suitable after five consecutive photocatalytic tests.

Author contribution statement

W. V.; A. C.; and C. D-U.: Conceived and designed the experiments; Analyzed and interpreted the data; Contributed reagents, materials, analysis tools or data; Wrote the paper. A. C.: Conceived and designed the experiments; Performed the experiments; Analyzed and interpreted the data; Contributed reagents, materials, analysis tools or data; Wrote the paper.

Data availability

The data used to support the findings of this study can be made available by the corresponding author upon request.

Declaration of competing interest

The authors declare that they have no known competing financial interests or personal relationships that could have appeared to influence the work reported in this paper.

Acknowledgements

The authors thank Universidad del Atlántico for the financial support.

Appendix A. Supplementary data

Supplementary data to this article can be found online at https://doi.org/10.1016/j.heliyon.2023.e20809.

References

[1] Y. Zhang, B. Zhou, H. Chen, R. Yuan, Heterogeneous photocatalytic oxidation for the removal of organophosphorus pollutants from aqueous solutions: a review, Sci. Total Environ. 856 (2023), 159048, https://doi.org/10.1016/J.SCITOTENV.2022.159048.
[2] H. Wang, X. Li, X. Zhao, C. Li, X. Song, P. Zhang, P. Huo, A review on heterogeneous photocatalysis for environmental remediation: from semiconductors to modification strategies, Chin. J. Catal. 43 (2022) 178–214, https://doi.org/10.1016/S1872-2067(21)63910-4.
[3] C.G. Thomson, A.L. Lee, F. Vilela, Heterogeneous photocatalysis in flow chemical reactors, Beilstein J. Org. Chem. 16 (2020) 1495, https://doi.org/10.3762/BJOC.16.125.
[4] S. Dong, J. Feng, M. Fan, Y. Pi, L. Hu, X. Han, M. Liu, J. Sun, J. Sun, Recent developments in heterogeneous photocatalytic water treatment using visible light-responsive photocatalysts: a review, RSC Adv. 5 (2015) 14610–14630, https://doi.org/10.1039/C4RA13734E.
[5] M. Sharma, A. Yadav, M.K. Mandal, K.K. Dubey, TiO2 based photocatalysis: a valuable approach for the removal of pharmaceuticals from aquatic environment, Int. J. Environ. Sci. Technol. 20 (2022) 4569–4584, https://doi.org/10.1007/S13762-021-03894-Y/METRICS.
[6] F. He, W. Jeon, W. Choi, Photocatalytic air purification mimicking the self-cleaning process of the atmosphere, Nat. Commun. 121 (2021) 12, https://doi.org/10.1038/s41467-021-22839-0, 2021) 1–4.
[7] K.P. Gopinath, N.V. Madhav, A. Krishnan, R. Malolan, G. Rangarajan, Present applications of titanium dioxide for the photocatalytic removal of pollutants from water: a review, J. Environ. Manag. 270 (2020), 110906, https://doi.org/10.1016/j.jenvman.2020.110906.
[8] D. Chen, Y. Cheng, N. Zhou, P. Chen, Y. Wang, K. Li, S. Huo, P. Cheng, P. Peng, R. Zhang, L. Wang, H. Liu, Y. Liu, R. Ruan, Photocatalytic degradation of organic pollutants using TiO2-based photocatalysts: a review, J. Clean. Prod. 268 (2020), 121725, https://doi.org/10.1016/J.JCLEPRO.2020.121725.
[9] Q. Li, Y. Wang, J. Liu, W. Kong, B. Ye, Structural and magnetic properties in Mn-doped ZnO films prepared by pulsed-laser deposition, Appl. Surf. Sci. 289 (2014) 42–46, https://doi.org/10.1016/J.APSUSC.2013.10.081.
[10] M. Ahmadi, M. Abrari, M. Ghanaatshoar, An all-sputtered photovoltaic ultraviolet photodetector based on co-doped CuCrO2 and Al-doped ZnO heterojunction, Sci. Rep. 111 (2021) 11, https://doi.org/10.1038/s41598-021-98273-5 (2021) 1–10.
[11] G. Gordillo, J.C. Pena, Development of system to grow ZnO films by plasma assisted reactive evaporation with improved thickness homogeneity for using in solar cells, J. Mater. Res. Technol. 19 (2022) 1191–1202, https://doi.org/10.1016/J.JMRT.2022.05.101.
[12] S.N. Fatimah Hasim, M.A. Abdul Hamid, R. Shamsudin, A. Jalar, Synthesis and characterization of ZnO thin films by thermal evaporation, J. Phys. Chem. Solid. 70 (2009) 1501–1504, https://doi.org/10.1016/J.JPCS.2009.09.013.
[13] T. Nguyen, N. Valle, J. Guillot, J. Bour, N. Adjeroud, Y. Fleming, M. Guennou, J.N. Audinot, B. El Adib, R. Joly, D. Arl, G. Frache, J. Polesel-Maris, Elucidating the growth mechanism of ZnO films by atomic layer deposition with oxygen gas via isotopic tracking, J. Mater. Chem. C 9 (2021) 4307–4315, https://doi.org/10.1039/D0TC05439A.
[14] S. Goktas, A. Goktas, A comparative study on recent progress in efficient ZnO based nanocomposite and heterojunction photocatalysts: a review, J. Alloys Compd. 863 (2021), 158734, https://doi.org/10.1016/J.JALLCOM.2021.158734.
[15] F. Tsin, A. Venerosy, J. Vidal, S. Collin, J. Clatot, L. Lombez, M. Paire, S. Borensztajn, C. Broussillou, P.P. Grand, S. Jaime, D. Lincot, J. Rousset, Electrodeposition of ZnO window layer for an all-atmospheric fabrication process of chalcogenide solar cell, Sci. Rep. 51 (2015) 5, https://doi.org/10.1038/srep08961 (2015) 1–8.
[16] N.C. Vega, B. Straube, O. Marin-Ramirez, D. Comedi, Low temperature chemical vapor deposition as a sustainable method to obtain c-oriented and highly UV luminescent ZnO thin films, Mater. Lett. 333 (2023), 133684, https://doi.org/10.1016/J.MATLET.2022.133684.
[17] S.P. Ratnayake, J. Ren, E. Colusso, M. Guglielmi, A. Martucci, E. Della Gaspera, S.P. Ratnayake, J. Ren, E. Della Gaspera, E. Colusso, M. Guglielmi, A. Martucci, SILAR deposition of metal oxide nanostructured films, Small 17 (2021), 2101666, https://doi.org/10.1002/SMLL.202101666.
[18] K.H. Maria, P. Sultana, M.B. Asfia, Chemical bath deposition of aluminum doped zinc sulfide thin films using non-toxic complexing agent: effect of aluminum doping on optical and electrical properties, AIP Adv. 10 (2020), 65315, https://doi.org/10.1063/5.0011191.
[19] D. Hu, X. Liu, S. Deng, Y. Liu, Z. Feng, B. Han, Y. Wang, Y. Wang, Structural and optical properties of Mn-doped ZnO nanocrystalline thin films with the different dopant concentrations, Phys. E Low-Dimensional Syst. Nanostructures. 61 (2014) 14–22, https://doi.org/10.1016/J.PHYSE.2014.03.007.
[20] M. Hassan, Y. Zhao, B. Xie, Employing TiO2 photocatalysis to deal with landfill leachate: current status and development, Chem. Eng. J. 285 (2016) 264–275, https://doi.org/10.1016/J.CEJ.2015.09.093.
[21] C.B. Ong, L.Y. Ng, A.W. Mohammad, A review of ZnO nanoparticles as solar photocatalysts: synthesis, mechanisms and applications, Renew. Sustain. Energy Rev. 81 (2018) 536–551, https://doi.org/10.1016/J.RSER.2017.08.020.

[22] P. Dhiman, G. Rana, A. Kumar, G. Sharma, D.V.N. Vo, M. Naushad, ZnO-based heterostructures as photocatalysts for hydrogen generation and depollution: a review, Environ. Chem. Lett. 2021 202 20 (2022) 1047–1081, https://doi.org/10.1007/S10311-021-01361-1.

[23] K.V.A. Kumar, B. Lakshminarayana, D. Suryakala, C. Subrahmanyam, Reduced graphene oxide supported ZnO quantum dots for visible light-induced simultaneous removal of tetracycline and hexavalent chromium, RSC Adv. 10 (2020) 20494–20503, https://doi.org/10.1039/D0RA02062A.

[24] R.S. Shinde, S.D. Khairnar, M.R. Patil, V.A. Adole, P.B. Koli, V.V. Deshmane, D.K. Halwar, R.A. Shinde, T.B. Pawar, B.S. Jagdale, A.V. Patil, Synthesis and characterization of ZnO/CuO nanocomposites as an effective photocatalyst and gas sensor for environmental remediation, J. Inorg. Organomet. Polym. Mater. 323 (2021) 1045–1066, https://doi.org/10.1007/S10904-021-02178-9, 32 (2022).

[25] A. Sułek, B. Pucelik, J. Kuncewicz, G. Dubin, J.M. Dąbrowski, Sensitization of TiO2 by halogenated porphyrin derivatives for visible light biomedical and environmental photocatalysis, Catal. Today 335 (2019) 538–549, https://doi.org/10.1016/j.cattod.2019.02.070.

[26] M.I. Litter, E. San Román, M.A. Grela, J.M. Meichtry, H.B. Rodríguez, Sensitization of TiO 2 by dyes: a way to extend the range of photocatalytic activity of TiO 2 to the visible region, in: Visible Light. Photocatal., Wiley-VCH Verlag GmbH & Co. KGaA, Weinheim, Germany, 2018, pp. 253–282, https://doi.org/10.1002/9783527808175.ch10.

[27] E. Regulska, D. Rivera-Nazario, J. Karpinska, M. Plonska-Brzezinska, L. Echegoyen, Zinc porphyrin-functionalized fullerenes for the sensitization of titania as a visible-light active photocatalyst: river waters and wastewaters remediation, Molecules 24 (2019) 1118, https://doi.org/10.3390/molecules24061118.

[28] C. Diaz-Uribe, F. Duran, W. Vallejo, E. Puello, X. Zarate, E. Schott, Photocatalytic study of TiO2 thin films modified with Anderson-type polyoxometalates (Cr, Co and Ni): experimental and DFT study, Polyhedron 231 (2023), 116253, https://doi.org/10.1016/J.POLY.2022.116253.

[29] H. Yasmeen, A. Zada, S. Ali, I. Khan, W. Ali, W. Khan, M. Khan, N. Anwar, A. Ali, A.M. Huerta-Flores, F. Subhan, Visible light-excited surface plasmon resonance charge transfer significantly improves the photocatalytic activities of ZnO semiconductor for pollutants degradation, J. Chinese Chem. Soc. 67 (2020) 1611–1617, https://doi.org/10.1002/JCCS.202000205.

[30] T.C. Bharat, Shubham, S. Mondal, H.S. Gupta, P.K. Singh, A.K. Das, Synthesis of doped zinc oxide nanoparticles: a review, mater, Today Proc 11 (2019) 767–775, https://doi.org/10.1016/J.MATPR.2019.03.041.

[31] S.B.A. Hamid, S.J. Teh, C.W. Lai, Photocatalytic water oxidation on ZnO: a review, Catalysts 7 (2017) 93, https://doi.org/10.3390/catal7030093.

[32] A.E. Ramírez, M. Montero-Muñoz, L.L. López, J.E. Ramos-Ibarra, J.A.H. Coaquira, B. Heinrichs, C.A. Páez, Significantly enhancement of sunlight photocatalytic performance of ZnO by doping with transition metal oxides, Sci. Rep. 111 (2021) 11, https://doi.org/10.1038/s41598-020-78568-9 (2021) 1–9.

[33] H. Bouzid, M. Faisal, F.A. Harraz, S.A. Al-Sayari, A.A. Ismail, Synthesis of mesoporous Ag/ZnO nanocrystals with enhanced photocatalytic activity, Catal. Today 252 (2015) 20–26, https://doi.org/10.1016/J.CATTOD.2014.10.011.

[34] O. Altintas Yildirim, H. Arslan, S. Sönmezoğlu, Facile synthesis of cobalt-doped zinc oxide thin films for highly efficient visible light photocatalysts, Appl. Surf. Sci. 390 (2016) 111–121, https://doi.org/10.1016/J.APSUSC.2016.08.069.

[35] K. Qi, X. Xing, A. Zada, M. Li, Q. Wang, S. yuan Liu, H. Lin, G. Wang, Transition metal doped ZnO nanoparticles with enhanced photocatalytic and antibacterial performances: experimental and DFT studies, Ceram. Int. 46 (2020) 1494–1502, https://doi.org/10.1016/J.CERAMINT.2019.09.116.

[36] E.J. Martinez-Finley, S. Chakraborty, M. Aschner, Manganese in biological systems, Encycl. Met. (2013) 1297–1303, https://doi.org/10.1007/978-1-4614-1533-6_284.

[37] J.E. Johnson, S.M. Webb, C. Ma, W.W. Fischer, Manganese mineralogy and diagenesis in the sedimentary rock record, Geochem. Cosmochim. Acta 173 (2016) 210–231, https://doi.org/10.1016/J.GCA.2015.10.027.

[38] J. Elanchezhiyan, K.P. Bhuvana, N. Gopalakrishnan, T. Balasubramanian, Investigation on Mn doped ZnO thin films grown by RF magnetron sputtering, Mater. Lett. 62 (2008) 3379–3381, https://doi.org/10.1016/J.MATLET.2008.03.013.

[39] E. Pragna, M. Ramanadha, A. Sudharani, K.S. Kumar, Nano synthesis and characterization of Co and Mn Co-doped ZnO by solution combustion technique, J. Supercond. Nov. Magnetism 34 (2021) 1507–1516, https://doi.org/10.1007/S10948-021-05874-2/METRICS.

[40] X. Li, X. Zhu, K. Jin, D. yang, Study on structural and optical properties of Mn-doped ZnO thin films by sol-gel method, Opt. Mater. 100 (2020), 109657, https://doi.org/10.1016/J.OPTMAT.2020.109657.

[41] R. Baghdad, B. Kharroubi, A. Abdiche, M. Bousmaha, M.A. Bezzerrouk, A. Zeinert, M. El Marssi, K. Zellama, Mn doped ZnO nanostructured thin films prepared by ultrasonic spray pyrolysis method, Superlattice. Microst. 52 (2012) 711–721, https://doi.org/10.1016/J.SPMI.2012.06.023.

[42] C. Manoharan, G. Pavithra, S. Dhanapandian, P. Dhamodharan, Effect of in doping on the properties and antibacterial activity of ZnO films prepared by spray pyrolysis, Spectrochim. Acta. A. Mol. Biomol. Spectrosc. 149 (2015) 793–799, https://doi.org/10.1016/J.SAA.2015.05.019.

[43] E. Jeyasingh, K.A. Charles, P. Thangaraj, K. Chandrasekaran, M.R. Viswanathan, Effect of Mn doping on the structural, optical, magnetic properties, and antibacterial activity of ZnO nanospheres, J. Sol. Gel Sci. Technol. 102 (2022) 357–371, https://doi.org/10.1007/S10971-022-05778-0/METRICS.

[44] M.L.A. Aguilera, J.M.F. Márquez, M.A.G. Trujillo, Y.M. Kuwahara, G.R. Morales, O.V. Galán, Influence of CdS thin films growth related with the substrate properties and conditions used on CBD technique, in: Energy Procedia, Elsevier, 2014, pp. 111–117, https://doi.org/10.1016/j.egypro.2013.12.016.

[45] A. Goktas, I.H. Mutlu, Y. Yamada, E. Celik, Influence of pH on the structural optical and magnetic properties of Zn1−xMnxO thin films grown by sol–gel method, J. Alloys Compd. 553 (2013) 259–266, https://doi.org/10.1016/J.JALLCOM.2012.11.097.

[46] A. Das, R.R. Wary, R.G. Nair, Mn-doped ZnO:Role of morphological evolution on enhanced photocatalytic performance, Energy Rep. 6 (2020) 737–741, https://doi.org/10.1016/J.EGYR.2019.11.148.

[47] J. Singh, A. Rathi, M. Rawat, V. Kumar, K.H. Kim, The effect of manganese doping on structural, optical, and photocatalytic activity of zinc oxide nanoparticles, Composites, Part B 166 (2019) 361–370, https://doi.org/10.1016/J.COMPOSITESB.2018.12.006.

[48] W. Vallejo, C. Diaz-Uribe, Á. Cantillo, Methylene blue photocatalytic degradation under visible irradiation on TiO2 thin films sensitized with Cu and Zn tetracarboxy-phthalocyanines, J. Photochem. Photobiol. Chem. 299 (2015) 80–86, https://doi.org/10.1016/J.JPHOTOCHEM.2014.11.009.

[49] W. Vallejo, A. Cantillo, C. Díaz-Uribe, Methylene blue photodegradation under visible irradiation on Ag-doped ZnO thin films, Int. J. Photoenergy 2020 (2020), https://doi.org/10.1155/2020/1627498.

[50] I.K. Konstantinou, T.A. Albanis, TiO 2 -assisted photocatalytic degradation of azo dyes in aqueous solution: kinetic and mechanistic investigations A review, Appl. Catal. B Environ. 49 (2004) 1–14, https://doi.org/10.1016/j.apcatb.2003.11.010.

[51] M. Samadi, M. Zirak, A. Naseri, E. Khorashadizade, A.Z. Moshfegh, Recent progress on doped ZnO nanostructures for visible-light photocatalysis, Thin Solid Films 605 (2016) 2–19, https://doi.org/10.1016/J.TSF.2015.12.064.

[52] E. Nowak, M. Szybowicz, A. Stachowiak, W. Koczorowski, D. Schulz, K. Paprocki, K. Fabisiak, S. Los, A comprehensive study of structural and optical properties of ZnO bulk crystals and polycrystalline films grown by sol-gel method, Appl. Phys. Mater. Sci. Process 126 (2020) 1–12, https://doi.org/10.1007/S00339-020-03711-2/TABLES/2.

[53] F. Friedrich, N.H. Nickel, Resonant Raman scattering in hydrogen and nitrogen doped ZnO, Appl. Phys. Lett. 91 (2007), 111903, https://doi.org/10.1063/1.2783222.

[54] J. Sann, J. Stehr, A. Hofstaetter, D.M. Hofmann, A. Neumann, M. Lerch, U. Haboeck, A. Hoffmann, C. Thomsen, Zn interstitial related donors in ammonia-treated ZnO powders, Phys. Rev. B 76 (2007), 195203, https://doi.org/10.1103/PhysRevB.76.195203.

[55] F. Friedrich, M.A. Gluba, N.H. Nickel, Identification of nitrogen and zinc related vibrational modes in ZnO, Appl. Phys. Lett. 95 (2009), https://doi.org/10.1063/1.3243454/338094.

[56] D.N. Montenegro, V. Hortelano, O. Martínez, M.C. Martínez-Tomas, V. Sallet, V. Muñoz-Sanjosé, J. Jiménez, Non-radiative recombination centres in catalyst-free ZnO nanorods grown by atmospheric-metal organic chemical vapour deposition, J. Phys. D Appl. Phys. 46 (2013), 235302, https://doi.org/10.1088/0022-3727/46/23/235302.

[57] J.B. Wang, G.J. Huang, X.L. Zhong, L.Z. Sun, Y.C. Zhou, E.H. Liu, Raman scattering and high temperature ferromagnetism of Mn-doped ZnO nanoparticles, Appl. Phys. Lett. 88 (2006), https://doi.org/10.1063/1.2208564/330962.

[58] S. Guo, Z. Du, S. Dai, Analysis of Raman modes in Mn-doped ZnO nanocrystals, Phys. Status Solidi. 246 (2009) 2329–2332, https://doi.org/10.1002/PSSB.200945192.

[59] V. Strelchuk, O. Kolomys, S. Rarata, P. Lytvyn, O. Khyzhun, C.O. Chey, O. Nur, M. Willander, Raman submicron spatial mapping of individual Mn-doped ZnO nanorods, Nanoscale Res. Lett. 12 (2017) 1–11, https://doi.org/10.1186/S11671-017-2127-4/FIGURES/10.

[60] K. Samanta, S. Dussan, R.S. Katiyar, P. Bhattacharya, Structural and optical properties of nanocrystalline Zn1-x Mnx O, Appl. Phys. Lett. 90 (2007), https://doi.org/10.1063/1.2751593/333614.

[61] E. Muchuweni, T.S. Sathiaraj, H. Nyakotyo, Synthesis and characterization of zinc oxide thin films for optoelectronic applications, Heliyon 3 (2017), e00285, https://doi.org/10.1016/j.heliyon.2017.e00285.

[62] A. López-Suárez, D. Acosta, C. Magaña, F. Hernández, Optical, structural and electrical properties of ZnO thin films doped with Mn, J. Mater. Sci. Mater. Electron. 31 (2020) 7389–7397, https://doi.org/10.1007/S10854-019-02830-8/METRICS.

[63] F. Mikailzade, H. Türkan, F. Önal, M. Zarbali, A. Göktaş, A. Tumbul, Structural and magnetic properties of polycrystalline Zn1−xMnxO films synthesized on glass and p-type Si substrates using Sol–Gel technique, Appl. Phys. Mater. Sci. Process 127 (2021) 1–8, https://doi.org/10.1007/S00339-021-04519-4/METRICS.

[64] F. Mikailzade, H. Türkan, F. Önal, Karataş, S. Kazan, M. Zarbali, A. Göktaş, A. Tumbul, Structural, optical and magnetic characterization of nanorod-shaped polycrystalline Zn1−xMnxO films synthesized using sol–gel technique, Appl. Phys. Mater. Sci. Process 126 (2020) 1–6, https://doi.org/10.1007/S00339-020-03953-0/METRICS.

[65] X. Wang, L. Sø, R. Su, S. Wendt, P. Hald, A. Mamakhel, C. Yang, Y. Huang, B.B. Iversen, F. Besenbacher, The influence of crystallite size and crystallinity of anatase nanoparticles on the photo-degradation of phenol, J. Catal. 310 (2014) 100–108, https://doi.org/10.1016/J.JCAT.2013.04.022.

[66] S. Ramachandran, J. Narayan, J.T. Prater, Effect of oxygen annealing on Mn doped ZnO diluted magnetic semiconductors, Appl. Phys. Lett. 88 (2006), https://doi.org/10.1063/1.2213930/911070.

[67] M.K. Lima, D.M. Fernandes, M.F. Silva, M.L. Baesso, A.M. Neto, G.R. de Morais, C.V. Nakamura, A. de Oliveira Caleare, A.A.W. Hechenleitner, E.A.G. Pineda, Co-doped ZnO nanoparticles synthesized by an adapted sol–gel method: effects on the structural, optical, photocatalytic and antibacterial properties, J. Sol. Gel Sci. Technol. 72 (2014) 301–309, https://doi.org/10.1007/s10971-014-3310-z.

[68] U. Holzwarth, N. Gibson, The Scherrer equation versus the "Debye-Scherrer equation,", Nat. Nanotechnol. 69 (2011) https://doi.org/10.1038/nnano.2011.145, 6 (2011) 534–534.

[69] S. Balamurali, S. Saravanakumar, R. Chandramohan, P.N. Magudeswaran, SILAR technique–grown Mn-doped ZnO thin films, Braz. J. Phys. 51 (2021) 1501–1508, https://doi.org/10.1007/S13538-021-00953-0/METRICS.

[70] Q. Ni, H. Cheng, J. Ma, Y. Kong, S. Komarneni, Efficient degradation of orange II by ZnMn2O4 in a novel photo-chemical catalysis system, Front. Chem. Sci. Eng. 146 (2020) 956–966, https://doi.org/10.1007/S11705-019-1907-Z, 14 (2020).

[71] J. Zhou, A. Dong, L. Du, C. Yang, L. Ye, X. Wang, L. Zhao, Q. Jiang, Mn-doped ZnO microspheres as cathode materials for aqueous zinc ion batteries with ultrastability up to 10 000 cycles at a large current density, Chem. Eng. J. 421 (2021), 127770, https://doi.org/10.1016/J.CEJ.2020.127770.

[72] S. Ben Yahia, L. Znaidi, A. Kanaev, J.P. Petitet, Raman study of oriented ZnO thin films deposited by sol–gel method, Spectrochim. Acta Part A Mol. Biomol. Spectrosc. 71 (2008) 1234–1238, https://doi.org/10.1016/J.SAA.2008.03.032.

[73] A.M. Toufiq, R. Hussain, A. Shah, A. Mahmood, A. Rehman, A. Khan, S. ur Rahman, The influence of Mn doping on the structural and optical properties of ZnO nanostructures, Phys. B Condens. Matter 604 (2021), 412731, https://doi.org/10.1016/J.PHYSB.2020.412731.

[74] D.K. Sharma, S. Shukla, K.K. Sharma, V. Kumar, A review on ZnO: fundamental properties and applications, Mater, Today Proc 49 (2022) 3028–3035, https://doi.org/10.1016/J.MATPR.2020.10.238.

[75] M.A.I. Molla, M. Furukawa, I. Tateishi, H. Katsumata, S. Kaneco, Studies of effects of calcination temperature on the crystallinity and optical properties of Ag-doped ZnO nanocomposites, J. Compos. Sci. 3 (2019) 18, https://doi.org/10.3390/JCS3010018, 18. 3 (2019).

[76] E.L. Simmons, Relation of the Diffuse reflectance remission function to the fundamental optical parameters, Opt. Acta Int. J. Opt. 19 (1972) 845–851, https://doi.org/10.1080/713818505.

[77] S. Agarwal, L.K. Jangir, K.S. Rathore, M. Kumar, K. Awasthi, Morphology-dependent structural and optical properties of ZnO nanostructures, Appl. Phys. Mater. Sci. Process 125 (2019) 1–7, https://doi.org/10.1007/S00339-019-2852-X/METRICS.

[78] K. Umar, A. Aris, T. Parveen, J. Jaafar, Z. Abdul Majid, A. Vijaya Bhaskar Reddy, J. Talib, Synthesis, characterization of Mo and Mn doped ZnO and their photocatalytic activity for the decolorization of two different chromophoric dyes, Appl. Catal. Gen. 505 (2015) 507–514, https://doi.org/10.1016/J.APCATA.2015.02.001.

[79] M. Ahmad, E. Ahmed, W. Ahmed, A. Elhissi, Z.L. Hong, N.R. Khalid, Enhancing visible light responsive photocatalytic activity by decorating Mn-doped ZnO nanoparticles on graphene, Ceram. Int. 40 (2014) 10085–10097, https://doi.org/10.1016/J.CERAMINT.2014.03.184.

[80] Y. Yang, Y. Li, L. Zhu, H. He, L. Hu, J. Huang, F. Hu, B. He, Z. Ye, Shape control of colloidal Mn doped ZnO nanocrystals and their visible light photocatalytic properties, Nanoscale 5 (2013), 10461, https://doi.org/10.1039/c3nr03160h.

[81] N.A. Putri, V. Fauzia, S. Iwan, L. Roza, A.A. Umar, S. Budi, Mn-doping-induced photocatalytic activity enhancement of ZnO nanorods prepared on glass substrates, Appl. Surf. Sci. 439 (2018) 285–297, https://doi.org/10.1016/J.APSUSC.2017.12.246.

[82] S. Dolabella, A. Borzì, A. Dommann, A. Neels, S. Dolabella, A. Borzì, A. Dommann, A. Neels, Lattice strain and defects analysis in nanostructured semiconductor materials and devices by high-resolution X-ray diffraction: theoretical and practical aspects, Small Methods 6 (2022), 2100932, https://doi.org/10.1002/SMTD.202100932.

[83] B.M. Rajbongshi, S.K. Samdarshi, Cobalt-doped zincblende–wurtzite mixed-phase ZnO photocatalyst nanoparticles with high activity in visible spectrum, Appl. Catal. B Environ. 144 (2014) 435–441, https://doi.org/10.1016/J.APCATB.2013.07.048.

[84] M. Pérez-González, S.A. Tomás, J. Santoyo-Salazar, S. Gallardo-Hernández, M.M. Tellez-Cruz, O. Solorza-Feria, Sol-gel synthesis of Ag-loaded TiO2-ZnO thin films with enhanced photocatalytic activity, J. Alloys Compd. 779 (2019) 908–917, https://doi.org/10.1016/J.JALLCOM.2018.11.302.

[85] S. Jun Park, G. Sankar Das, F. Schütt, R. Adelung, Y. Kumar Mishra, K. Malika Tripathi, T. Kim, Visible-light photocatalysis by carbon-nano-onion-functionalized ZnO tetrapods: degradation of 2,4-dinitrophenol and a plant-model-based ecological assessment, Asia Mater 11 (2019) 1–13, https://doi.org/10.1038/s41427-019-0107-0.

[86] Ş.Ş. Türkyılmaz, N. Güy, M. Özacar, Photocatalytic efficiencies of Ni, Mn, Fe and Ag doped ZnO nanostructures synthesized by hydrothermal method: the synergistic/antagonistic effect between ZnO and metals, J. Photochem. Photobiol. Chem. 341 (2017) 39–50, https://doi.org/10.1016/J.JPHOTOCHEM.2017.03.027.

[87] W. Vallejo, A. Cantillo, B. Salazar, C. Diaz-Uribe, W. Ramos, E. Romero, M. Hurtado, Comparative study of ZnO thin films doped with transition metals (Cu and Co) for methylene blue photodegradation under visible irradiation, Catalysts 10 (2020) 528, https://doi.org/10.3390/catal10050528.

[88] S. Jayswal, R.S. Moirangthem, Construction of a solar spectrum active SnS/ZnO p–n heterojunction as a highly efficient photocatalyst: the effect of the sensitization process on its performance, New J. Chem. 42 (2018) 13689–13701, https://doi.org/10.1039/C8NJ02098A.